©2025 IEEE. Personal use of this material is permitted. Permission from IEEE must be obtained for all other uses, in any current or future media, including reprinting/republishing this material for advertising or promotional purposes, creating new collective works, for resale or redistribution to servers or lists, or reuse of any copyrighted component of this work in other works.

A Low-Profile Dual-Band Self-Decoupled Shared-Aperture Patch Antenna Array for 6G Beamforming

Xichen Wang, Can Ding, *Senior Member, IEEE*, Shiyong Li, *Senior Member, IEEE*, Shang-Yi Sun, *Graduate Student Member, IEEE*, Chunyang Teng, Guoqiang Zhao, and Houjun Sun

***Abstract*—This paper presents a dual-band shared-aperture patch antenna array with self-decoupling capability. A patch unit is first proposed, comprising four square patches and a Jerusalem cross-shaped stripe (JS), all located on the same PCB layer. The unit operates in the high-band (HB) mode by individually exciting any of the four patches, and in the low-band (LB) mode by exciting the central JS, which in turn excites the entire unit. The two operating bands exhibit a small frequency ratio of 1.2:1, enabling coverage of adjacent 6G mid-bands. Both in-band and cross-band isolations exceed 20 dB across all ports, without requiring additional decoupling structures. To demonstrate scalability, four units are cascaded to form a larger array. Small T-shaped stripes, also printed on the same layer, are introduced to enhance isolation between HB patches nested in different units, while the units maintain self-decoupling in the LB. Both the patch unit and the array are fabricated and tested. The measured results agree well with simulations, validating the proposed design. The array operates in two bands: the LB centered at 12 GHz with an 14.2% bandwidth, and the HB centered at 14.5 GHz with a 11% bandwidth. Beam-scanning ranges of ±50° in the HB mode and ±20° in the LB mode are achieved. With its structural simplicity, low profile, self-decoupling capability within both bands, and robust beamforming performance, the proposed array serves as a promising phased array candidate for future 6G applications.**

***Index Terms*—Beamforming, differentially-fed antenna, dual-band, self-decoupling, shared-aperture antenna, sixth-generation (6G) wireless communication.**

I. Introduction

With the evolution from 3G to 6G, communication equipment, including base stations and vehicle-mounted devices, must support multiple communication standards and diverse user scenarios [1]-[5]. Driven by the continuous pursuit of antenna miniaturization, the "aperture sharing" concept has been adopted, enabling multiple antennas to operate at different frequency bands within a shared aperture [6]-[10]. This approach enhances space utilization efficiency and enables multifunctional antenna systems. However, it also presents a significant challenge: mitigating multiple types of interference between antenna elements.

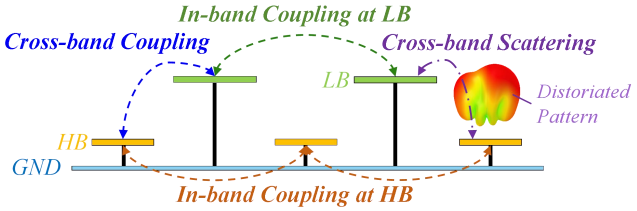

Fig. 1 Illustration of the interference mechanisms within a typical side-by-side dual-band antenna array.

As shown in Fig. 1, a typical side-by-side shared-aperture dual-band array suffers from severe scattering and coupling [11]–[25]. On one hand, the taller low-band (LB) antennas scatter the electromagnetic fields radiated by the lower high-band (HB) antennas, significantly distorting their radiation patterns—often the most critical issue in such configurations. Conversely, the HB antennas can also reduce the gain of the LB antennas under certain conditions [11]. These distortions are collectively referred to as cross-band scattering. On the other hand, strong coupling effects further degrade performance, reducing port-to-port isolation. These include in-band coupling between the HB antennas, in-band coupling between the LB antennas, and cross-band coupling between antennas operating at different frequency bands. They should be addressed differently and simultaneously.

Cross-band scattering occurs when one antenna obstructs another's radiation, and various mitigation strategies have been explored. One approach modifies the LB antenna to be electromagnetically transparent to HB radiation [12]-[15]. Another lifts the HB antennas to the same height or above the LB antennas to prevent obstruction [16]-[22]. But all these designs have a profile comparable to or exceeding the standard dipole height at the LB. In [23], the LB antenna's profile is reduced without elevating the HB antenna, achieving a lower array profile, but this approach is limited to a single LB-HB pair and lacks array applicability.

If both LB and HB antennas are patch antennas placed on the same layer, blocking and cross-scattering effects are minimum, and the profile is much lower than existing designs. However, no effective shared-aperture patch configuration currently

This work was supported by the National Natural Science Foundation of China under Grant 62371043. (corresponding author: Shiyong Li)

Xichen Wang, Shiyong Li, Chunyang Teng, Guoqiang Zhao, and Houjun Sun are with the Beijing Key Laboratory of Millimeter Wave and Terahertz Technology, Beijing Institute of Technology (BIT), Beijing 100081, China. They are also with the Tangshan Research Institute of BIT, Tangshan 063007, China (e-mail: lisy_98@bit.edu.cn).

Can Ding and Shang-yi Sun are with the Global Big Data Technologies Center (GBDTC), University of Technology Sydney (UTS), Ultimo, NSW 2007, Australia (e-mail: Can.Ding@uts.edu.au).

exists, as such an arrangement leads to severe coupling issues. Although existing shared-aperture antenna designs also address coupling issues, different types of coupling are typically managed separately, and not all three types shown in Fig. 1 are mitigated simultaneously. This can significantly impact beamforming performance when integrated into a larger array. Moreover, one of the key objectives of shared-aperture antennas is miniaturization. Ideally, the decoupling network should occupy minimal space to preserve the compactness of the antenna structure. This presents an inherent contradiction, making the design challenge even more demanding.

To achieve decoupling between antennas without occupying additional space, the self-decoupling method [24]-[31] offers a promising solution. In [24]-[26], self-decoupling of single-band antenna arrays is implemented by designing weak-field structures. Recently, several self-decoupled dual-band shared-aperture antenna designs have been published [13], [15], [27]-[31]. However, these approaches typically achieve decoupling in only one frequency band, usually by incorporating supplementary structures within the antennas operating in the other band. There is currently no self-decoupling method that manages couplings in both the bands for shared-aperture antennas.

In this paper, a compact and low-profile self-decoupled dual-band shared-aperture patch array is developed, as illustrated in Fig. 2. The HB antennas are standard square patches, highlighted in yellow, operating in the 13.7-15.3 GHz band (11%). Four HB patches, along with a Jerusalem cross-shaped stripe (JS) highlighted in green, form an LB element, which operates in the 11-12.7 GHz band (14.2%). The in-band isolation between HB elements, the in-band isolation between LB elements, and the cross-band isolation between LB and HB antennas all exceed 20 dB across both frequency bands, without requiring additional decoupling structures. Since the LB and HB antennas are located on the same layer, the antennas maintain a stable radiation pattern without cross-band scattering. These characteristics guarantee a superior beamforming capability of the array. To validate the proposed design, an array consisting of a 1×4 LB array and a 2×8 HB array is fabricated and tested. The results demonstrate favorable beam-scanning performance in both bands, achieving scanning ranges of ±20° for the LB and ±50° for the HB.

The novelty and contribution of this work are summarized as follows:

(1) **New shared-aperture antenna design method with small frequency ratio:** This method enables aperture sharing on the same PCB layer for both LB and HB designs with a small frequency ratio, effectively avoiding cross-band scattering. Although such co-layered aperture sharing typically increases coupling, all coupling levels in the proposed array are maintained below –20 dB.

(2) **New dual-band self-decoupling method**: This work develops a self-decoupling approach that effectively operates in two frequency bands. The in-band coupling at both LB and HB, as well as the cross-band coupling between them, are self-managed.

(3) **Ultra-compact structure and low profile**: This work has an ultra-low profile of only 0.089 λ_L. The combination of space-saving strategies—aperture-sharing and self-decoupling, advances antenna miniaturization to the next level.

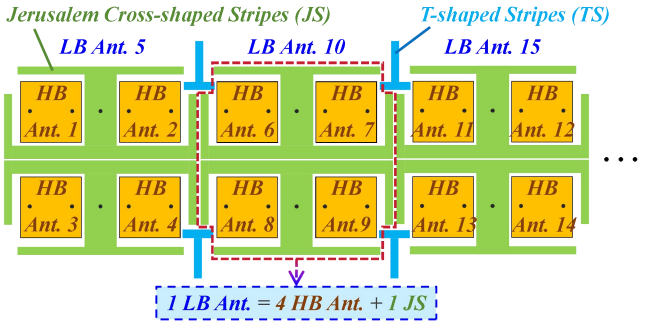

Fig. 2. Configuration of the developed self-decoupled shared-aperture patch antenna array. The yellow square patches represent the HB antennas, while four HB antennas, together with the green Jerusalem cross-shaped stripes (JS), form the LB antenna.

(4) **Application in 6G**: The antenna is designed to operate at two adjacent 6G mid-bands with a small frequency ratio. The well-maintained isolation and stable radiation patterns enable robust beamforming performance. Combined with its scalability, compactness, and structural simplicity, the array serves as a promising phased array candidate for 6G systems.

The rest of the paper is organized as follows: Section II discusses the operating and decoupling mechanisms of a shared-aperture unit comprising one LB antenna and four HB antennas. Section III extends this unit to a larger array, focusing on inter-unit coupling. Section IV presents the experimental results, and Section V concludes the paper.

II. Shared-Aperture Patch Unit

According to [32], the 6G spectrum is expected to encompass mid-range frequencies from 7 to 15 GHz, including specific bands such as 10.7-13.25 GHz and 14-15.35 GHz. Consequently, the HB and LB antennas in this paper are designed to operate at center frequencies of 14.5 GHz and 12 GHz, respectively, for 6G applications. Fig. 3 illustrates the configuration evolvement of the developed dual-band shared-aperture patch unit. All patches are printed on the top of a Rogers 5880 substrate with a thickness of 2 mm, dielectric constant of 2.2, and a loss tangent of 0.0009. Each unit is differentially excited using a pair of probes, which are combined into a single port via a differential power divider.

As shown in Fig. 3(a), the **initial configuration** (Config.) is a conventional 2×2 patch array operating at targeted HB centered at 14.5 GHz. To enable operation in the LB centered at 12 GHz, **Config. 2** introduces a cross-shaped stripe. By exciting this stripe, the HB array can also operate in a low-band mode, allowing the unit to support both LB and HB operation. However, this configuration suffers from strong coupling among the ports. In **Config. 3**, the cross-shaped stripe is extended into a JS structure, which significantly enhances both in-band and cross-band isolations. Finally, in **Config. 4**, a slot is etched into the JS, further improving the cross-band isolation and improving the LB operating bandwidth. The design insights and rationale behind each evolutionary step are discussed in detail below.

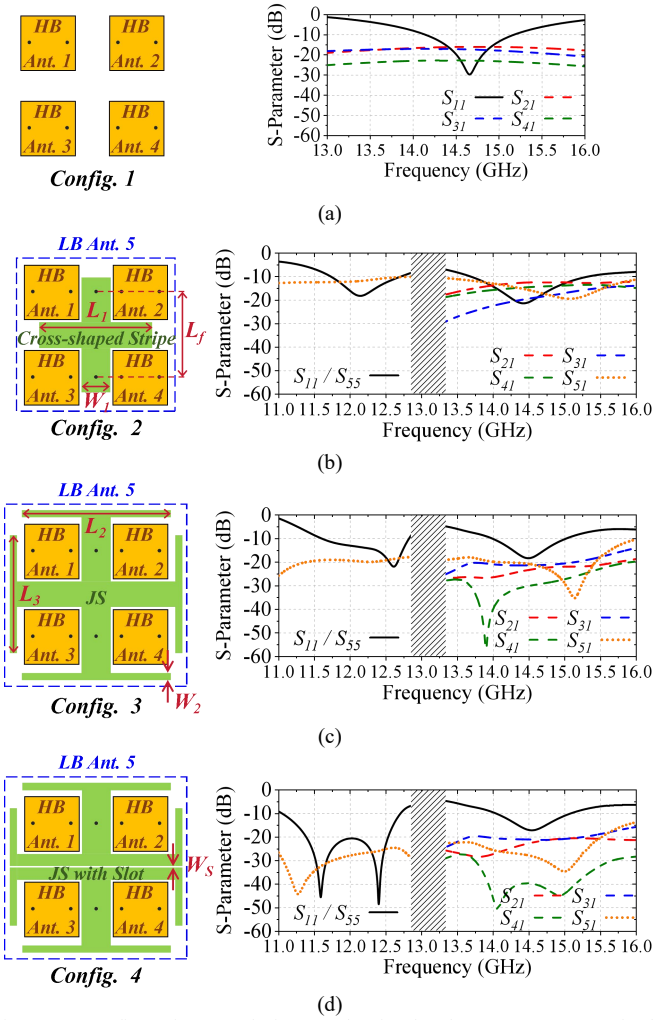

Fig. 3. Configuration evolution and simulated S-parameters of the shared-aperture antenna unit. (a) Config. 1. (b) Config. 2. (c) Config. 3. (d) Config. 4. (Reflection coefficients, in-band coupling coefficients, and cross-band coupling are plotted in solid, dash, and dot lines, respectively.)

A. Config. 1: Standard 2×2 square patch array

As shown in Fig. 3(a), Config. 1 is a standard patch antenna array, where each element has a size of 0.3 λ_H × 0.3 λ_H mm^2 (λ_H is the wavelength at the HB center frequency of 14.5 GHz) and is horizontally polarized. The center-to-center spacing between elements is 0.5 λ_H, and edge-to-edge distance is 0.19 λ_H. The patches are impedance-matched across a bandwidth from 14.3 to 15.3 GHz, corresponding to a fractional bandwidth of 6.9%. The in-band couplings among the four patches are strong, remaining above –20 dB, and includes both E-plane coupling (e.g., between Ants. 1 and 2) and H-plane coupling (e.g., between Ants. 1 and 3).

B. Config. 2: Excite the HB array in the LB mode

In Config. 2, as shown in Fig. 3(b), a cross-shaped stripe is integrated with the patches. Similar structures are commonly used in magneto-electric (ME) dipole designs [33]-[36], where the cross-shaped stripe forms part of the feed network to excite four dipoles operating in the half-wavelength mode. However, in this work, the structure is repurposed to excite the four patch elements, and the operating principle is different. When the unit is excited via the cross-shaped stripe, it does not resonate in the half-wavelength mode typical of ME dipoles, nor in the fundamental TM_{10} mode of the entire unit behaving as a single patch. If either of those modes were excited, the resulting operating frequency would be much lower, yielding a frequency ratio between the HB and LB modes exceeding 2:1. Our target is to excite the entire unit in a LB mode around 12 GHz, corresponding to a small frequency ratio of approximately 1.2:1 relative to the HB center frequency of 14.5 GHz. This requires a different strategy from those typically used to achieve dual-band operation with a 2:1 frequency ratio.

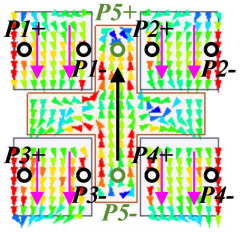

Fig. 4. Surface current distribution of Config. 2 when the unit is excited in the LB mode at 12 GHz.

Fig. 4 illustrates the surface current distribution when the unit is excited through the ports (*P5*+ and *P5*−) on the cross-shaped stripe. As shown, all four patches are simultaneously excited and resonate in the TM_{10} mode. However, since the excitation occurs through the cross-shaped stripe, the current path is longer than that of individual patch excitation via the HB ports (*P1*+ and *P1*−), shifting the resonant frequency down to approximately 12 GHz. If the entire unit was to behave as a single large patch, the expected operating frequency would drop further to around 6 GHz. The resonance frequency of the LB mode can be simply adjusted by changing the length of the stripe (L_1).

Although Config. 2 demonstrates the potential for dual-mode operation within a single unit, it suffers from strong in-band and cross-band coupling, as shown in Fig. 3(b), which must be mitigated.

C. Config. 3: Improving isolations using JS

As illustrated in Fig. 3(c), Config. 3 replaces the original cross-shaped stripe with the JS, which significantly enhanced both the in-band and cross-band isolations. The JS was optimized to meet the following three goals simultaneously.

In-band isolation between the HB antennas: The in-band isolations between any two HB antennas exceed 20 dB, including both E-plane coupled pairs and H-plane coupled pairs. The decoupling mechanism is widely used in many decoupling designs [37], where an additional coupling path is introduced such that the coupled energy from the new path destructively interferes with that from the original path, effectively cancelling out the mutual coupling. This decoupling mechanism, commonly adopted in many decoupling designs [37], introduces an additional coupling path—typically via a parasitic element (JS)—so that the energy coupled through this new path destructively interferes with that of the original coupling path, thereby effectively suppressing the overall mutual coupling.

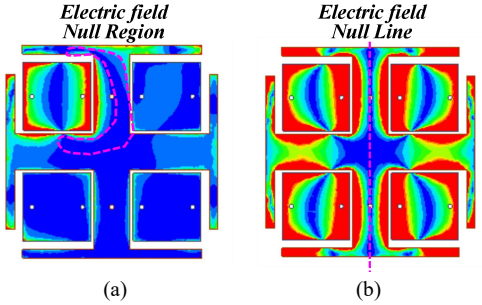

Fig. 5. Electric field distributions on the unit when (a) the HB Ant. 1 is excited and (b) all the HB antennas are excited.

Cross-band isolation at the HB: Fig. 5(a) shows the electric field distribution on the unit when the HB Ant. 1 is excited. As seen in the figure, a null region of the electric field appears on the JS. This null region can be tuned by optimizing the size of the JS and the distance between the JS and the HB patches. Similar null regions are observed when the other HB antennas are excited. These null regions overlap, as illustrated in Fig. 5(b). By placing the feed ports of the LB antenna within this overlapped region, high cross-band isolation at the HB can be achieved [38].

Cross-band isolation at the LB: When the shared-aperture unit is excited in the LB mode via *P5*, all HB patches are simultaneously excited, as demonstrated by the current distributions in Fig. 6 for either Configs. 2, 3, or 4. This inevitably leads to energy coupling into the HB ports, resulting in strong cross-band coupling. However, since the HB patches are fed differentially, a potential solution is to balance the coupling currents entering the two differential ports. Specifically, if the currents entering *P1*+ and *P1*− are equal in both amplitude and phase, they will cancel each other out at the combined port *P1* after passing through the differential power divider (PD).

Fig. 6 plots the magnitudes and phases of S_{51+} and S_{51-}, representing the energy coupled from the LB port *P5* into the differential HB ports *P1*+ and *P1*−. It also includes the magnitude of S_{51}, which characterizes the net energy reaching port *P1* after ideal combination through a differential PD.

In Config. 2, as shown in Fig. 6(a), the magnitudes of S_{51+} and S_{51-} are relatively low (–20 to –25 dB); however, they exhibit a 180-degree phase difference. This causes the coupled energy entering the two differential ports to add constructively at the combined port, resulting in a high S_{51} value of around –10 dB. In contrast, Config. 3, illustrated in Fig. 6(b), achieves a much smaller phase difference between S_{51+} and S_{51-}, allowing partial cancellation at the combined port and thereby suppressing S_{51} to approximately –20 dB.

It is worth noting that the magnitude and phase balance between S_{51+} and S_{51-} can be fine-tuned by adjusting the lengths of the JS arms—L_2 for amplitude and L_3 for phase. In theory, one could achieve perfect cancellation ($S_{51} = S_{51+} + S_{51-} = 0$) by carefully optimizing these parameters, thereby maximizing cross-band isolation. However, such tuning would impact other critical performance metrics, such as in-band coupling. For this reason, further suppression of S_{51} is not pursued in Config. 3, but is instead realized in Config. 4.

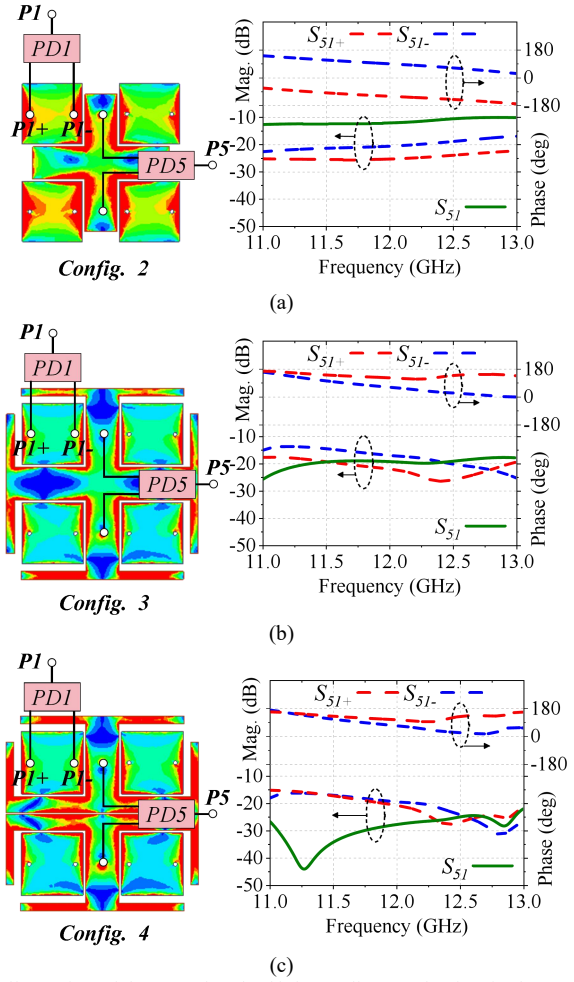

Fig. 6. Illustration of the cross-band self-decoupling mechanism in the LB mode when port *P5* is excited, along with the simulated transmission coefficients from the LB combined port *P5* to the HB differential ports *P1*+ and *P1*−, and to the summed port P1, for (a) Config. 2, (b) Config. 3, and (c) Config. 4.

D. Config. 4: Further decoupling and LB bandwidth enhancement by etching slot on the JS

As shown in Fig. 3(d), Config. 4 introduces a narrow slot on the JS to further enhance performance, including the cross-band isolations and the LB mode bandwidth of the unit. Comparing Fig. 6(c) with Fig. 6(b), it is observed that the phase difference between S_{51+} and S_{51-} remains largely unchanged after introducing the narrow slot. However, the magnitude balance improves significantly. Prior to adding the slot, the coupling to *P1*+ is weaker than to *P1*-, as *P1*+ is located farther from the vertical arm of the JS. The narrow slot facilitates strong horizontal current flow, which redirects more energy toward *P1*+. This redistribution enhances the amplitude balance between S_{51+} and S_{51-}, a critical requirement for effective decoupling.

As illustrated in Fig. 6(c), S_{51} is suppressed to as low as –45 dB when both the amplitudes and phases of S_{51+} and S_{51-} are nearly identical. As frequency increases, amplitude and phase imbalances, particularly the phase difference, gradually grow, leading to increased cross-band coupling. S_{51} peaks around 12.7 GHz, where the phase difference between S_{51+} and S_{51-} is the largest, further validating the proposed cross-band

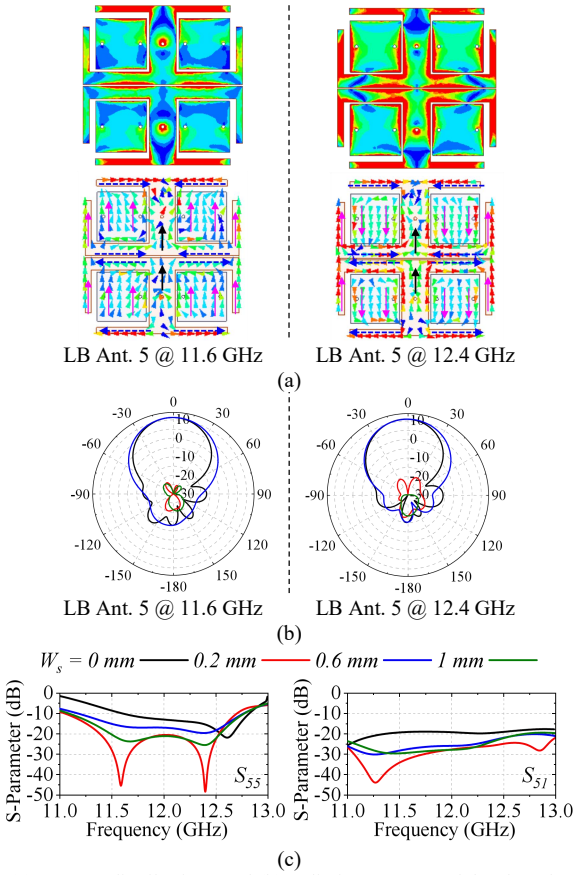

Fig. 7. (a) Current distributions and (b) radiation patterns of the shared-aperture unit in Config. 4 when the LB mode is excited at 11.6 GHz and 12.4 GHz; and the (c) variation of S_{55} and S_{51} with the different values of W_S.

self-decoupling analysis.

On the other hand, the LB operational bandwidth is significantly widened from 10% (11.6–12.8 GHz) in Config. 3 to 14.3% (11–12.7 GHz) in Config. 4. This improvement is primarily attributed to better impedance matching at the first resonance around 11.6 GHz. As shown in Fig. 3(d), Config. 4 clearly exhibits two well-defined resonances, whereas Config. 3 also has two, but the first one is poorly matched. Figs. 7(a) and 7(b) compare the current distribution and radiation patterns of the unit at these two resonances. Despite some reversed surface currents observed at the second resonance, the unit maintains consistent radiation patterns and realized gain, i.e., 11 dBi at 11.6 GHz and 11.3 dBi at 12.4 GHz. The matching at the first resonance can be effectively tuned by adjusting the slot width, as demonstrated by the parameter sweep results shown in Fig. 7(c).

E. Final configuration

The final configuration of the developed small frequency ration, dual-band shared-aperture unit is presented in Fig. 8. The entire structure consists of three substrate layers and three metal layers. All radiators are printed on the top side of *Sub 1*. The bottom side of *Sub 3* accommodates the differential power dividers required for differentially-fed antennas (DFAs). The top side of *Sub 2* serves as the ground plane. Feed probes extend through all layers, facilitating the connection between the feed network at the bottom and the radiating patches at the

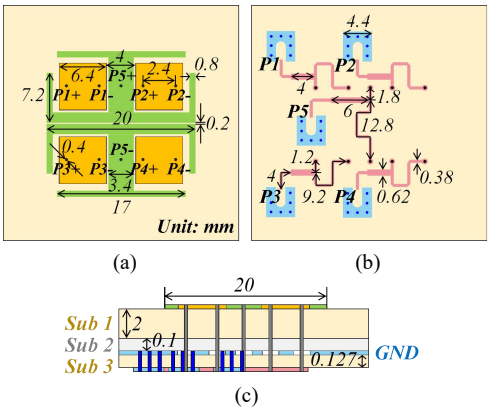

Fig. 8. (a) Top view, (b) bottom view, and (c) side view of the developed dual-band shared-aperture patch antenna unit consisting of one LB antenna and four HB antennas. (Unit: millimeter)

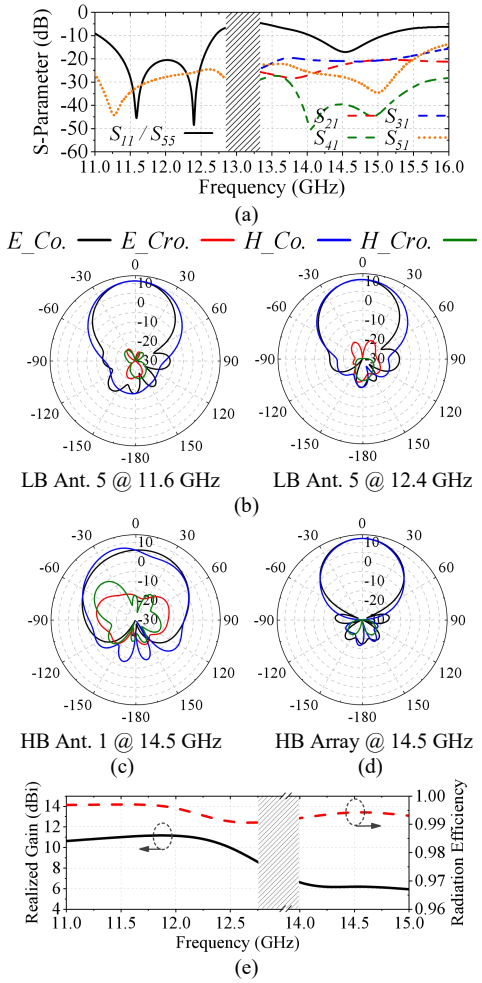

Fig. 9. Simulated results of the final configuration of the developed shared-aperture unit. (a) S-parameter results; (b) radiation pattern of LB Ant. 5 at two sample LB frequencies; (c) radiation pattern of HB Ant. 1 at the HB center frequency; (d) radiation pattern of the HB array (Ants. 1+2+3+4) at the HB center frequency, and (e) realized gain and radiation efficiency.

top. *Sub 1* and *Sub 3* are made of Rogers 5580. *Sub 2* acts as a prepreg layer, utilizing Rogers 4450F prepreg, which has a dielectric constant of 3.2 and a loss tangent of 0.004. The dimension of the final unit is 20×20×2.227 mm^3, corresponding to $0.8\lambda_L \times 0.8\lambda_L \times 0.089\lambda_L$ (λ_L is the wavelength at the LB center frequency of 12 GHz).

The simulated S-parameter results of the developed unit, including the differential PDs, are shown in Fig. 9(a). The unit operates in both the LB mode from 11 to 12.7 GHz (14.3%) and the HB mode from 14 to 15.1 GHz (7.6%). The isolation between any two ports across both LB and HB bands exceeds 20 dB. Fig. 9(b) plots the E- and H-plane radiation patterns of the unit in the LB mode at 11.6 GHz and 12.4 GHz, showing realized gains ranging from 10.5 to 11.3 dBi across the LB band. Fig. 9(c) presents the radiation patterns of HB Ant. 1 at the HB center frequency of 14.5 GHz. As depicted in Fig. 9(e), the realized gain ranges from 5.8 to 6.3 dBi across the HB band, while the radiation efficiency remains high, ranging from 99.3% to 99.7%. Other HB patches demonstrate similar performance due to the structural symmetry. Although the HB antenna exhibits lower gain compared to the LB antenna, this is because only one of the four HB patches is excited. When all four HB patches are excited simultaneously, the realized gain increases to 12 dBi, with the corresponding radiation patterns shown in Fig. 9(d).

III. Shared-Aperture Patch Array

As shown in Fig. 10, four of the shared-aperture patch units described in the previous section are cascaded to form a linear shared-aperture patch array, comprising a 2×8 HB array and a 1×4 LB array. The edge-to-edge spacing between adjacent units is only 0.8 mm, corresponding to approximately 0.03 λ_L. To enhance isolation between HB patches located in adjacent units, such as between Ants. 2 and 6, six additional T-shaped stripes (TS) are introduced. The adjacent LB antennas are self-decoupled by optimizing the JS.

A. Self-decoupling between adjacent LB antennas

To illustrate the patch unit's self-decoupling capability at the LB, Fig. 11 compares the current distributions and S-parameter results of arrays employing units with Configs. 2 and 4. Note that the results for the unit with Config. 3 are similar to those of Config. 4 and are therefore not presented here. As can be observed from the figure, strong coupling exists among adjacent units when the unit is excited using the cross-shaped strip (Config. 2). However, after replacing the cross-shaped strip with the JS (Config. 4), the coupling is significantly reduced, even though the edge-to-edge distance is smaller. The isolation exceeds 25 dB across the entire LB band. This demonstrates that the JS plays a critical role in confining the energy within each unit.

B. Decoupling adjacent HB antennas nested in different units

As discussed in the previous section, the in-band couplings between the HB antennas nested within the same shared-aperture unit (e.g., HB Ants. 1–4) are effectively mitigated by the JS. However, when multiple units are cascaded, the couplings between adjacent HB antennas from different units (e.g., between HB Ants. 2 and 6) remain sufficiently strong to impact the overall performance of the array. This problem is addressed by introducing TS pairs between adjacent patch units. As shown in Fig. 12, the inclusion of TS substantially suppresses the in-band coupling between any two

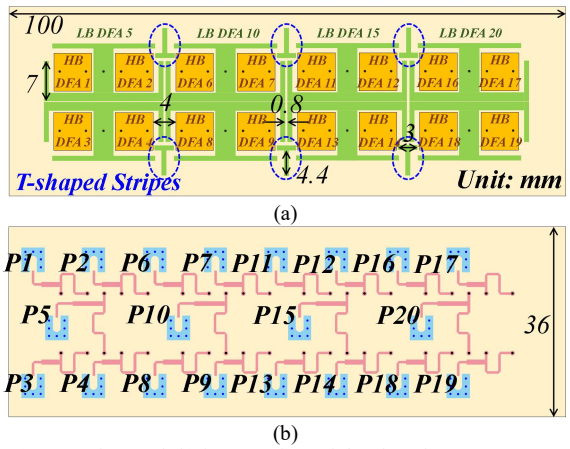

Fig. 10. (a) Top view and (b) bottom view of the shared-aperture antenna array consisting of a 2×8 HB array and a 1×4 LB array.

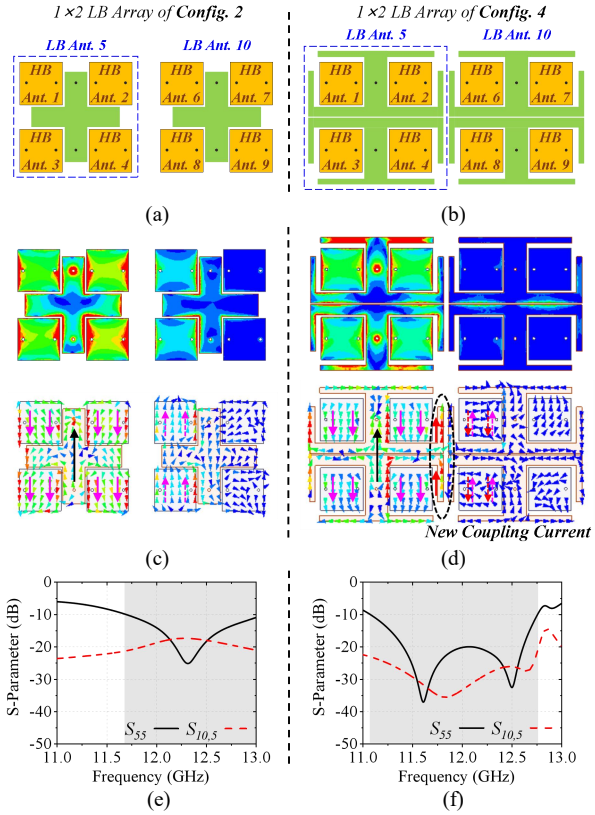

Fig. 11. (a), (b) Configurations; (c), (d) current distributions; and (e), (f) S-parameter results at the LB of Config.2 and Config.4, each employing different shared-aperture units.

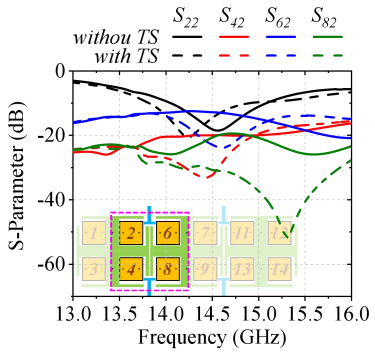

Fig. 12. Simulated S-parameters of the shared-aperture array without and with TS at the HB.

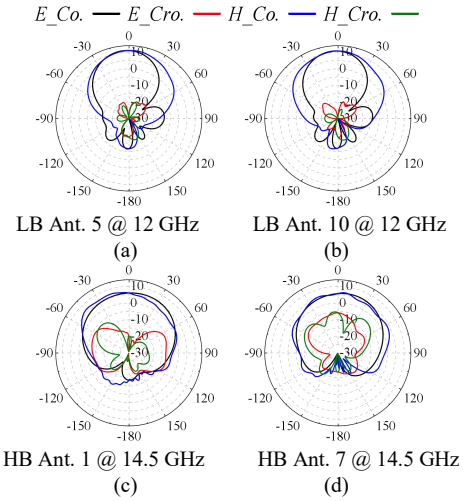

Fig. 13. Simulated radiation patterns. (a) LB Ant. 5 and (b) LB Ant. 10 at 12 GHz, (c) HB Ant. 1 and (d) HB Ant. 7 at 14.5 GHz.

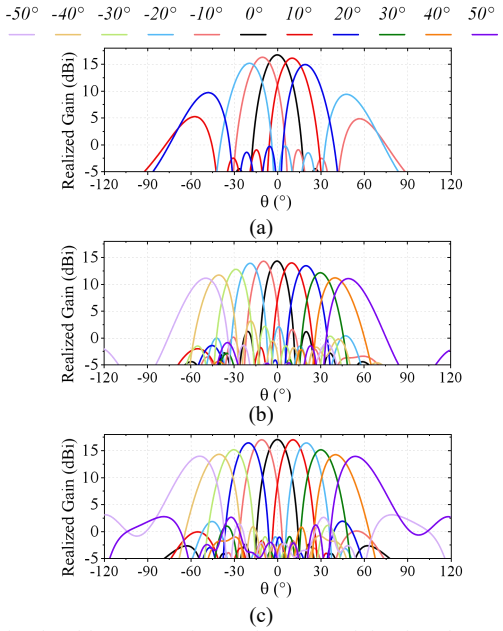

Fig. 14. Simulated beam scanning performance of the shared-aperture antenna array at (a) 12 GHz and at 14.5 GHz of the (b) 1×8 and (c) 2×8 array.

HB patches. Although a slight frequency shift of the HB antenna is observed, the operational band remains largely unchanged. Additionally, the TS structures have minimal impact on the cross-band coupling and the in-band coupling at the LB, preserving the overall isolation performance of the array.

C. *Beam scanning performances*

Fig. 13 shows the E- and H-plane radiation patterns of two HB antennas and two LB antennas located at different positions within the array. Despite a slight asymmetry observed in the HB patterns in the H-plane, which is primarily caused by the asymmetric current distribution on the JS, the overall radiation patterns remain well-formed. These antennas are subsequently employed for beamforming by applying progressive phase shifts at their feed ports.

The simulated beam-scanning performance of the shared-aperture antenna array is illustrated in Fig. 14. For the

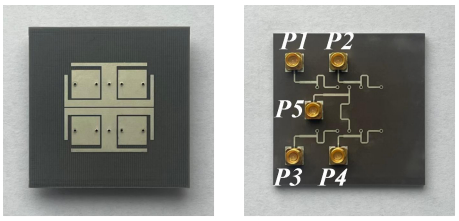

Fig. 15. (a) Top view and (b) bottom view of the fabricated prototype of the shared-aperture antenna unit.

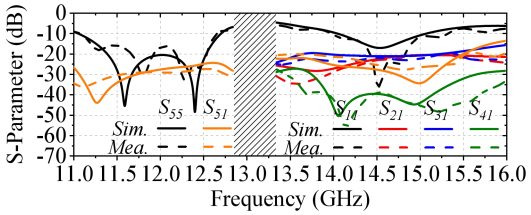

Fig. 16. Simulated and measured S-parameters of the shared-aperture antenna unit.

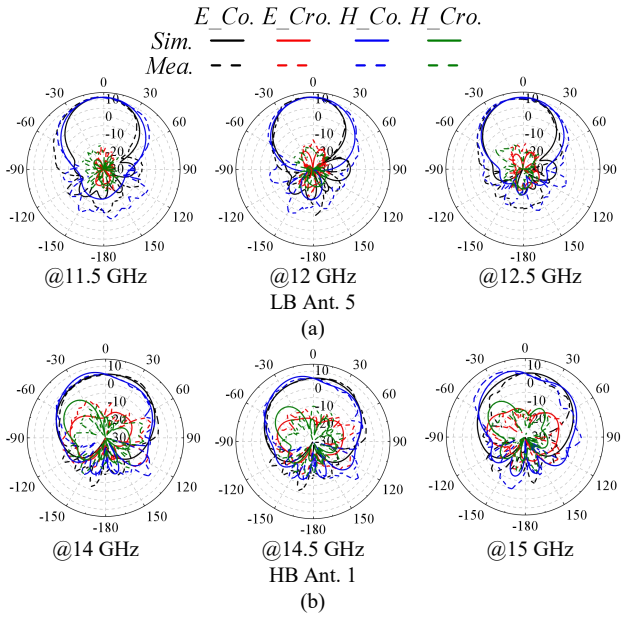

Fig. 17. Simulated and measured radiation patterns of the shared-aperture unit at (a) the LB and (b) the HB.

LB array, as shown in Fig. 14(a), beam steering within ±20° is achieved at 12 GHz, with the realized gain ranging from 15 dBi to 16.8 dBi. Fig. 14(b) presents the radiation patterns of the HB array comprising only the patches in the top row (HB Ant. 1, 2, 6, 7, 11, 12, 16, and 17). At 14.5 GHz, the HB beam can be steered within ±50°, achieving a peak gain of 14.3 dBi with a gain variation of only 2.8 dB. The bottom row patches exhibit similar performance and can operate as a separate array. When exciting the full 2×8 array, as shown in Fig. 14(c), the scanning performance in the horizontal plane is similar to that of the 1×8 array, while offering a higher peak gain of 17.0 dBi. On the other hand, the vertical beamwidth is narrower for the 2×8 array. For instance, at broadside (θ = 0°), the half-power beamwidth (HPBW) in the vertical plane is 13.6° for the 1×8 array and 13.9° for the 2×8 array. The scanning performance of the LB array is limited compared to the HB array due to the small number of elements (only four).

IV. Experimental Results

A. Shared-aperture antenna unit

The developed shared-aperture antenna unit was fabricated and tested, with the prototype shown in Fig. 15. Figs. 16 and 17 presents a comparison between the simulated and measured S-parameters and radiation patterns of the unit. The measured results show good agreement with the simulations. As shown in Fig. 16, the measured 10-dB impedance bandwidth of HB Ant. 1 spans from 13.9 to 15.3 GHz, corresponding to a 9.7 % fractional bandwidth, which is slightly wider than the simulated result. Within this band, the in-band coupling between the HB antennas is effectively suppressed to below –20 dB. On the other hand, the measured bandwidth of LB Ant. 5 is 14.2%, spanning from 11 to 12.7 GHz. Additionally, the measured cross-band coupling (S_{51}) is less than -25 dB within the LB band and less than -20 dB within the HB band. The results for the other HB antennas are similar due to the structural symmetry and are therefore not presented.

Fig. 17 presents the simulated and measured radiation patterns of HB Ant. 1 and LB Ant. 5 at three sample frequencies. The measured results closely match the simulated ones, validating the design. The measured realized gain of the HB antenna exceeds 6 dBi, while that of the LB antenna varies between 10 and 11.1 dBi.

B. Shared-aperture antenna array

The shared-aperture antenna array was also fabricated and tested, with a photo of the prototype shown in Fig. 18. The comparison between the simulated and measured S-parameter results of shared-aperture antenna array are plotted in Fig. 19. The measured results exhibit good agreement with the simulations, with the observed discrepancies primarily resulting from additional losses from the cables and SMP connectors.

As shown in Fig. 19(a), the measured bandwidth of the LB antennas is 14.2%, covering 11 GHz to 12.7 GHz, while the measured HB bandwidth spans from 13.7 GHz to 15.3 GHz, corresponding to 11%. Fig. 19(b) shows that the cross-band coupling between any HB and LB antennas remains below –21 dB across both bands.

Fig. 19(c) presents the in-band coupling coefficients between the LB antennas, all of which are lower than –22 dB, indicating strong isolation. The in-band coupling coefficients between adjacent HB antennas are lower than –26 dB at the center frequencies. It is noted that the coupling between HB antennas located in adjacent units, such as S_{62}, is relatively higher, staying above –16 dB across the entire band, while all other in-band couplings remain below –20 dB. This slight degradation in isolation is still acceptable for beamforming applications, especially considering the compactness and simplicity of the proposed structure.

Fig. 20 presents the simulated and measured radiation patterns of selected LB and HB antennas at representative frequencies. The measured radiation patterns are generally well-formed and align closely with the simulations. The measured realized gains of LB antennas range from 10.4 to 10.9 dBi, while those of the HB antennas vary from 5.6 to 6.8 dBi.

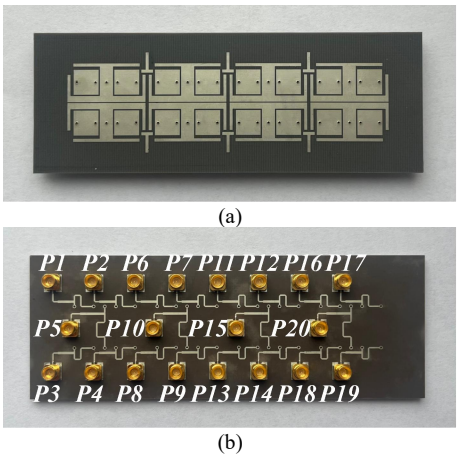

(a)

(b)

Fig. 18. (a) Top view and (b) bottom view of the fabricated prototype of the shared-aperture antenna array.

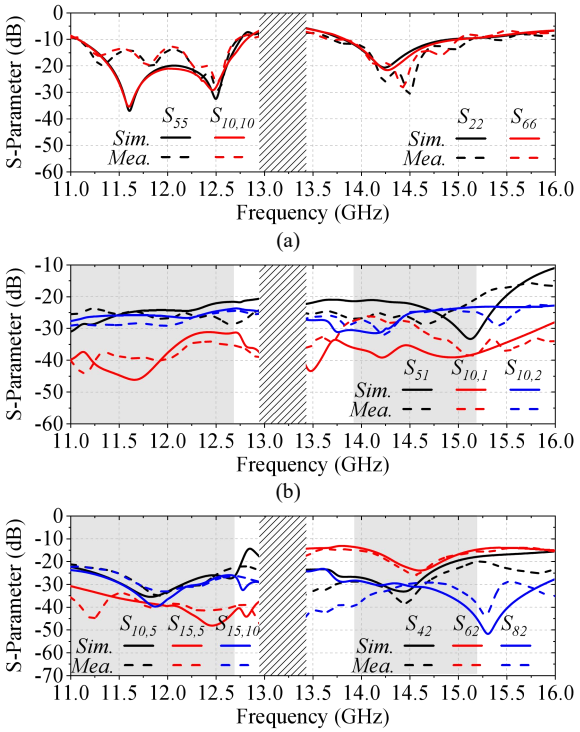

(a)

(b)

(c)

Fig. 19. Simulated and measured (a) reflected coefficients at both LB and HB, (b) cross-band coupling coefficients at both LB and HB, (c) in-band coupling coefficients at LB and HB.

Due to the lack of affordable beamformers, the beamforming performance of the array was evaluated in MATLAB using ideal phase shifts and the measured radiation patterns of individual elements, each measured separately while the other elements were terminated with 50-Ohm loads. The results are compared with the simulated performance in Fig. 21. The HB array achieves a peak gain of 14.6 dBi at boresight and supports beam scanning up to ±50° with a modest gain drop of 2.8 dB. It should be noted that these results correspond to the HB array in the top row only; if the bottom-row HB array is also excited, the overall gain can be further increased. Meanwhile, the LB array attains a scanning range of ±20° with a peak realized gain of 16.8 dBi and minimal gain fluctuation of only 0.7 dB.

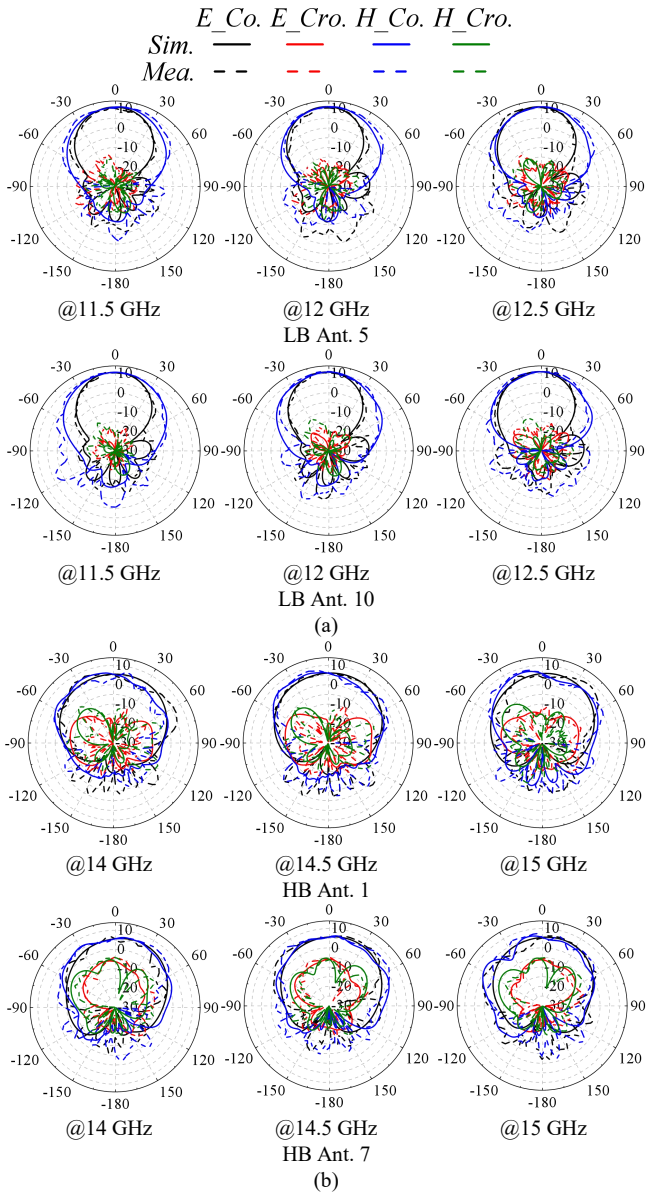

Fig. 20. Simulated and measured radiation patterns of (a) LB Ant. 5 an Ant. 10 and (b) HB Ant. 1 and Ant. 7 in the shared-aperture array at several sample frequencies.

However, noticeable differences are observed in the side lobe levels of the LB array between the simulated results and the measurement-based MATLAB synthesis. This discrepancy arises because the simulations account for both mutual coupling and active S-parameters, whereas the MATLAB-based synthesis considers only the coupling effects using unit-pattern synthesis and neglects impedance mismatch. To more accurately evaluate the beamforming performance of the self-decoupled shared-aperture antenna array, we fabricated three feed networks with different phase shift values: one for scanning the LB array to 20°, and two for scanning the HB array to 20° and 50°, respectively. The designs of the power dividers and the corresponding simulation and measurement results are presented in Fig. 22. Good agreement is observed between the simulated and measured beamforming patterns.

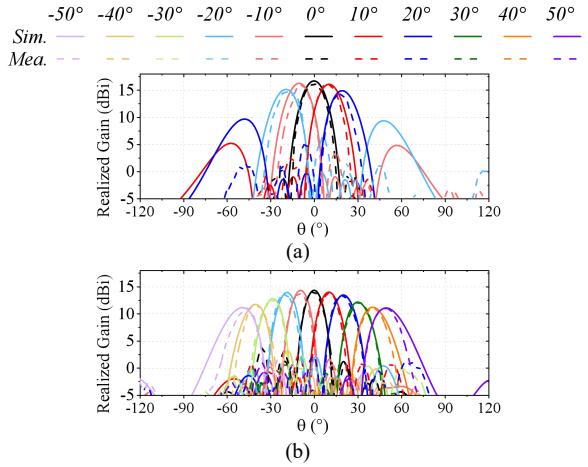

Fig. 21 Simulated and measured beamforming performance at (a) 12 GHz and (b) 14.5 GHz via MATLAB.

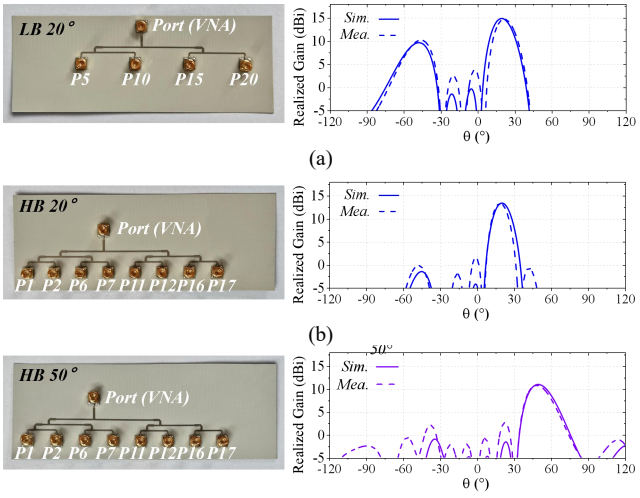

Fig. 22. Fabricated feed networks for beamforming measurement. (a) 20° of LB, (b) 20°, and (c) 50° of HB.

TABLE I
COMPARISON OF DUAL-BAND SHARED-APERTURE ANTENNA ARRAY DECOUPLING PERFORMANCE

Ref.	Method	ES	FR/BW	Profile	Scanning	Isolation
[13]	HB under LB	LB: Element HB: 0.51 λ_H	1.5:1 LB: 19% HB: 36%	0.22 λ_L	LB: NG HB: NG	LB: NG HB: >22 dB Cx: >25 dB
[20]	Cavity-backed Slots	LB: Element HB: 0.6 λ_H	4:1 LB: 33.3% HB: 32.7%	0.28 λ_L	LB: NG HB: NG	LB: NG HB: >26 dB Cx: >29 dB
[21]	Cavity-backed Slots	LB: 0.3 λ_L HB: 0.47 λ_H	4:1 LB: 33.3% HB: 32.7%	0.17 λ_L	LB: NG HB: NG	LB: >18 dB HB: >29 dB Cx: >25 dB
[30]	FSS	LB: 0.3 λ_L HB: 0.42 λ_H	1.5:1 LB: 40% HB: 14.1%	0.19 λ_L	LB: NG HB: NG	LB: >22 dB HB: >22 dB Cx: >20 dB
[31]	Branch + ODS	LB: Element HB: 0.41 λ_H	3.1:1 LB: 38% HB: 28%	0.28 λ_L	LB: NG HB: NG	LB: NG HB: >30 dB Cx: >25 dB
[40]	Metal Groove	LB: Element HB: 0.2 λ_H	7.4:1 LB: 11.7% HB: 11.9%	0.03 λ_L	LB: NG HB: ±25°	LB: NG HB: NG Cx: >15 dB
[41]	Metal Stripe	LB: 0.05 λ_L HB: 0.4 λ_H	2:1 LB: 9.3% HB: 26.9%	0.25 λ_L	LB: NG HB: ±60°	LB: >15 dB HB: >18 dB Cx: >16 dB
Our	**Self Decoupling**	**LB: 0.03 λ_L HB: 0.19 λ_H**	**1.2:1 LB: 14.2% HB: 11%**	**0.09 λ_L**	**LB: ±20° HB: ±50°**	**LB: >22 dB HB: >20 dB Cx: > 21 dB**

*Ref.: Reference; ES: Edge-to-edge Spacing; FR: Frequency Ratio; BW: Working Bandwidth; NG: Not Given.

C. Comparison

TABLE I presents a comparison with state-of-the-art dual-band shared-aperture antenna arrays. While the bandwidth achieved in this work is relatively narrower, this is primarily due to the use of microstrip patch elements, which offer significantly lower profiles. The proposed design introduces a novel self-decoupling method capable of operating in two frequency bands with a small frequency ratio. This self-decoupling method offers excellent simplicity and compactness. Furthermore, good beamforming performance has been validated, demonstrating its suitability for future 6G applications.

V. Conclusion

This paper presented a compact, low-profile dual-band shared-aperture patch antenna array with self-decoupling capability. The design process began with a standard patch array and evolved through the introduction of a Jerusalem cross (JS) and a slotted JS to enable dual-band operation with strong in-band and cross-band isolation. The decoupling mechanisms were analyzed in detail and validated through full-wave simulations. The unit was extended into a linear array, with additional T-shaped strips introduced to manage inter-unit coupling. Both the unit and array were fabricated and measured, showing good agreement with simulations. The results confirm the proposed structure's effectiveness in achieving high isolation, compact integration, and robust beamforming, making it a promising solution for future 6G antenna systems.

References

[1] A Vision of 6G Wireless Systems: Applications, Trends, Technologies, and Open Research Problems," *IEEE Netw.*, vol. 34, no. 3, pp. 134–142, May 2020.

[2] M. Na, J. Lee, G. Choi, T. Yu, J. Choi, J. Lee, and S. Bahk, ''Operator's perspective on 6G: 6G services, vision, and spectrum,'' *IEEE Commun. Mag.*, vol. 62, no. 8, pp. 178–184, Aug. 2024.

[3] D. Cuellar, M. Sallal and C. Williams, "BSM-6G: Blockchain-Based Dynamic Spectrum Management for 6G Networks: Addressing Interoperability and Scalability," *IEEE Access*, vol. 12, pp. 59643-59664, 2024.

[4] D. Jung et al., "Terahertz Antenna-in-Package Design and Measurement for 6G Communications Systems," *IEEE Trans. Antennas Propag.*, vol. 72, no. 2, pp. 1085-1096, Feb. 2024.

[5] X. Wang, C. Ding, G. Zhao, S. Li, Y. Chen and H. Sun, "Differential and Symmetrical Decoupling Network for Differentially Fed Antennas," *IEEE Antennas Wireless Propag. Lett.*, vol. 23, no. 3, pp. 1129-1133, March 2024.

[6] Xing-Yu Cheng, Can Ding, and Richard W. Ziolkowski, "Dual-Band Shared-Aperture Dielectric Resonator Antenna (DRA) with Suppressed Cross-Band Interactions", *IEEE Trans. Antennas Propag.,* vol. 72, no. 7, pp. 5694-5704, July 2024.

[7] Yi He, Can Ding, Chengxiang Chang, Gengming Wei, and Y. Jay Guo, "A Bowl-Shaped Filtering Antenna with Wideband Cross-Band Scattering Mitigation for Dual-Band Base Stations", *IEEE Trans. Antennas Propag.,* vol. 72, no. 8, pp. 6723-6728, Aug. 2024.

[8] H. -H. Sun, H. Zhu, C. Ding, B. Jones and Y. J. Guo, "Scattering Suppression in a 4G and 5G Base Station Antenna Array Using Spiral Chokes," *IEEE Antennas Wireless Propag. Lett*, vol. 19, no. 10, pp. 1818-1822, Oct. 2020.

[9] Y. He, C. Ding, G. Wei and Y. J. Guo, "An Embedded Scheme-Based Dual-band Shared Aperture Base Station Antenna Array," *2024 International Symposium on Antennas and Propagation (ISAP),* Incheon, Korea, Republic of, 2024.

[10] X. -Y. Cheng, C. Ding and R. W. Ziolkowski, "A Semi-Transmissive Cylindrical Metasurface Enabled Dual-Band Shared-Aperture DRA," *2024 International Symposium on Antennas and Propagation (ISAP)*, Incheon, Korea, Republic of, 2024.

[11] S. -Y. Sun, C. Ding, W. Jiang and Y. J. Guo, "Simultaneous Suppression of Cross-Band Scattering and Coupling Between Closely Spaced Dual-Band Dual-Polarized Antennas," *IEEE Trans. Antennas Propag.*, vol. 71, no. 8, pp. 6423-6434, Aug. 2023.

[12] H. -H. Sun, C. Ding, H. Zhu, B. Jones and Y. J. Guo, "Suppression of Cross-Band Scattering in Multiband Antenna Arrays," *IEEE Trans. Antennas Propag.*, vol. 67, no. 4, pp. 2379-2389, April 2019.

[13] X. Liu et al., "A Mutual-Coupling-Suppressed Dual-Band Dual-Polarized Base Station Antenna Using Multiple Folded-Dipole Antenna," *IEEE Trans. Antennas Propag.*, vol. 70, no. 12, pp. 11582-11594, Dec. 2022.

[14] X. W. Dai, D. L. Mi, H. Hong, S. Y. Lin and G. Q. Luo, "Dual-Polarized Antenna With Suppression of Cross-Band Scattering in Multiband Array," *IEEE Antennas Wireless Propag. Lett.*, vol. 20, no. 8, pp. 1592-1595, Aug. 2021.

[15] S. J. Yang and X. Y. Zhang, "Frequency Selective Surface-Based Dual-Band Dual-Polarized High-Gain Antenna," *IEEE Trans. Antennas Propag.*, vol. 70, no. 3, pp. 1663-1671, March 2022.

[16] Y. Zhu, Y. Chen, and S. Yang, "Decoupling and low-profile design of dual-band dual-polarized base station antennas using frequency-selective surface," *IEEE Trans. Antennas Propag.*, vol. 67, no. 8, pp. 5272–5281, Aug. 2019.

[17] Y. Chen, J. Zhao and S. Yang, "A Novel Stacked Antenna Configuration and its Applications in Dual-Band Shared-Aperture Base Station Antenna Array Designs," *IEEE Trans. Antennas Propag.*, vol. 67, no. 12, pp. 7234-7241, Dec. 2019.

[18] D. He, Y. Chen and S. Yang, "A Low-Profile Triple-Band Shared-Aperture Antenna Array for 5G Base Station Applications," *IEEE Trans. Antennas Propag.*, vol. 70, no. 4, pp. 2732-2739, April 2022.

[19] Y. Zhu, Y. Chen and S. Yang, "Integration of 5G Rectangular MIMO Antenna Array and GSM Antenna for Dual-Band Base Station Applications," *IEEE Access*, vol. 8, pp. 63175-63187, 2020.

[20] Y. Li and Q. -X. Chu, "Shared-Radiator Design of Dual-Band Coplanar Base Station Antenna Array Using Cavity-Backed Slots," *IEEE Trans. Antennas Propag.*, vol. 69, no. 12, pp. 8985-8990, Dec. 2021.

[21] Y. Li and Q. -X. Chu, "Coplanar Dual-Band Base Station Antenna Array Using Concept of Cavity-Backed Antennas," *IEEE Trans. Antennas Propag.*, vol. 69, no. 11, pp. 7343-7354, Nov. 2021.

[22] Askarian, P. Burasa and K. Wu, "Frequency-Diversified Space-Efficient Radiating Surface Using Convolved Electric and Magnetic Currents for Highly Dense Multiband Antenna-Frontend Integration," *Electromagn. Sci.*, vol. 2, no. 1, pp. 1-14, March 2024.

[23] Y. He, S. Wang, G. Wei, C. Ding and Y. Jay Guo, "A New Buffering Scheme for Shared-Aperture Dual-Band Base Station Antenna Array Utilizing Tight-Coupling Concept," *IEEE Trans. Antennas Propag.*, 2025.

[24] H. Lin, Q. Chen, Y. Ji, X. Yang, J. Wang and L. Ge, "Weak-Field-Based Self-Decoupling Patch Antennas," *IEEE Trans. Antennas Propag.*, vol. 68, no. 6, pp. 4208-4217, June 2020.

[25] Q. X. Lai, Y. M. Pan and S. Y. Zheng, "A Self-Decoupling Method for MIMO Antenna Array Using Characteristic Mode of Ground Plane," *IEEE Trans. Antennas Propag.*, vol. 71, no. 3, pp. 2126-2135, March 2023.

[26] K. -D. Hong, X. Zhang, H. -Y. Weng, L. Zhu and T. Yuan, "A 2-D Self-Decoupling Method Based on Antenna-Field Redistribution for MIMO Patch Antenna Array," *IEEE Antennas Wireless Propag. Lett.*, vol. 23, no. 3, pp. 940-944, March 2024.

[27] Y. Li and Q. -X. Chu, "Dual-Band Base Station Antenna Array Using the Low-Band Antenna as Parasitic Decoupler," *IEEE Antennas Wireless Propag. Lett.*, vol. 21, no. 7, pp. 1308-1312, July 2022.

[28] Y. Li and Q. -X. Chu, "Self-Decoupled Dual-Band Shared-Aperture Base Station Antenna Array," *IEEE Trans. Antennas Propag.*, vol. 70, no. 7, pp. 6024-6029, July 2022.

[29] S. J. Yang, R. Ma and X. Y. Zhang, "Self-Decoupled Dual-Band Dual-Polarized Aperture-Shared Antenna Array," *IEEE Trans. Antennas Propag.*, vol. 70, no. 6, pp. 4890-4895, June 2022.

[30] D. He, Q. Yu, Y. Chen and S. Yang, "Dual-Band Shared-Aperture Base Station Antenna Array With Electromagnetic Transparent Antenna Elements," *IEEE Trans. Antennas Propag.*, vol. 69, no. 9, pp. 5596-5606, Sept. 2021.

[31] R. Wu, J. -H. Lin, F. -C. Chen and L. H. Ye, "Dual-Broadband Aperture-Shared Base Station Antenna Array Using Double Decoupling

Techniques," *IEEE Antennas Wireless Propag. Lett.*, vol. 23, no. 10, pp. 3262-3266, Oct. 2024.
[32] J. Zhang, H. Miao, P. Tang, L. Tian and G. Liu, "New Mid-Band for 6G: Several Considerations from the Channel Propagation Characteristics Perspective," *IEEE Comm. Mag.*, vol. 63, no. 1, pp. 175-180, January 2025.
[33] Q. Xue, S. W. Liao and J. H. Xu, "A Differentially-Driven Dual-Polarized Magneto-Electric Dipole Antenna," *IEEE Trans. Antennas Propag.*, vol. 61, no. 1, pp. 425-430, Jan. 2013.
[34] M. Wang and C. H. Chan, "A Novel Differentially-Fed Dual-Polarized Shared Aperture Antenna Array," *IEEE Trans. Antennas Propag.*, vol. 70, no. 12, pp. 12276-12281, Dec. 2022.
[35] Q. Yang et al., "Millimeter-Wave Dual-Polarized Differentially Fed 2-D Multibeam Patch Antenna Array," *IEEE Trans. Antennas Propag.*, vol. 68, no. 10, pp. 7007-7016, Oct. 2020.
[36] L. Xiang et al., "A Wideband Differentially Fed Dual-Polarized Antenna Array for 5G/6G mmWave Application," *IEEE Antennas Wireless Propag. Lett.*, vol. 23, no. 2, pp. 903-907, Feb. 2024.
[37] W. Song, X. -W. Zhu, L. Wang and W. Hong, "Simple Structure E-Plane Decoupled Millimeter Wave Antenna Based on Current Cancellation Model," *IEEE Trans. Antennas Propag.*, vol. 70, no. 10, pp. 9871-9876, Oct. 2022.
[38] N. -W. Liu, Y. -D. Liang, L. Zhu, G. Fu, Y. Liu and Y. Yun, "Electric-Field Null Bending of a Single Dual-Port Patch Antenna for Colinear Polarization Decoupling Using Characteristic Modes Analysis," *IEEE Trans. Antennas Propag.*, vol. 70, no. 12, pp. 12247-12252, Dec. 2022.
[39] J. Jiang and Q. -X. Chu, "Broadband Decoupling for Antenna Arrays Using Multiple Decoupling Nulls," *IEEE Trans. Antennas Propag.*, vol. 71, no. 11, pp. 8616-8627, Nov. 2023.
[40] X. -H. Ding, W. -W. Yang, W. Qin and J. -X. Chen, "A Broadside Shared Aperture Antenna for (3.5, 26) GHz Mobile Terminals With Steerable Beam in Millimeter-Waveband," *IEEE Trans. Antennas Propag.*, vol. 70, no. 3, pp. 1806-1815, March 2022.
[41] G. -W. Yang and S. Zhang, "A Dual-Band Shared-Aperture Antenna With Wide-Angle Scanning Capability for Mobile System Applications," *IEEE Transactions on Vehicular Technology*, vol. 70, no. 5, pp. 4088-4097, May 2021.
[42] C. -X. Mao, S. Gao, Y. Wang, Q. Luo and Q. -X. Chu, "A Shared-Aperture Dual-Band Dual-Polarized Filtering-Antenna-Array With Improved Frequency Response," *IEEE Trans. Antennas Propag.*, vol. 65, no. 4, pp. 1836-1844, April 2017.
[43] A. Ali, M. Nabeel Awan, W. Ahmad Malik, S. Yaqoob Chaudhry, Hidayatullah and J. Haider, "A Compact and High Gain X/Ku Band Shared Aperture Antenna Array With Enhanced Inter-Band and Cross-Band Isolation," *IEEE Access*, vol. 12, pp. 146137-146146, 2024.

Xichen Wang received the bachelor's degree in North University of China, Shanxi, China, in 2022. She is currently enrolled in the five-year doctoral program in the School of Integrated Circuits and Electronics, Beijing Institute of Technology (BIT), Beijing, China. She received the Honorable Mention Awards and Travel Grants at IEEE APS 2024 and 2025, and the Best Paper Awards for IEEE iWRF&AT 2024 and IEEE IWS 2025. Her research interests include differentially-fed antenna, antenna decoupling, shared-aperture antenna technologies for 5G and 6G.

Can Ding (Senior Member, IEEE) received the bachelor's degree in integrated circuit and integrated system from Xidian University, Xi'an, China, in 2009, and the joint Ph.D. degree in electromagnetic fields and microwave technology from Xidian University and Macquarie University, Sydney, NSW, Australia, in 2016.

From 2015 to 2017, he was a Post-Doctoral Research Fellow with the University of Technology Sydney (UTS), Ultimo, NSW, Australia, where he is currently an Associate Professor with the Faculty of Engineering and IT (FEIT), and a Core Member of the Global Big Data Technologies Center (GBDTC). His accomplishments encompass several research and industry projects, patented innovations, and a portfolio of over 120 publications in top-tier journals and conferences.

He has been an ARC DECRA Fellow from 2020 to 2024. He has been serving as an Associate Editor of the IEEE Antennas and Wireless Propagation Letters (AWPL) since 2024. He was recognized as a Top Reviewer for the IEEE Transactions on Antennas and Propagation (TAP) for four consecutive years (2022–2025). He also received the distinction of Outstanding Reviewer for IEEE AWPL for three consecutive years (2023–2025) and was named an Outstanding Associate Editor in 2025. Since late 2023, he has been a member of the IEEE AP-S Education Committee and the EurAAP Working Group on Early Careers, and since 2025 he has also served on the IEEE AP-S Technical Committee 4 on Metamaterials. He was selected as a 2024 IEEE AP-S Young Professional Ambassador and has been serving on the IEEE AP-S Young Professional Committee since 2025.

Shiyong Li (Senior Member, IEEE) received the B.S. degree in electrical engineering from Shandong University, Jinan, China, in 2002, and the Ph.D. degree in electromagnetic field and microwave technology from the Beijing Institute of Technology, Beijing, China, in 2008. From 2009 to 2010, he was a Postdoctoral Researcher with the School of Electronics Engineering and Computer Science, Peking University, Beijing. Since 2010, he has been with the Faculty of the Beijing Institute of Technology, where he is currently a Professor. And He is also with the Tangshan Research Institute of BIT, Tangshan 063007, China. From 2017 to 2018, he was a Visiting Research Scholar with the Center for Advanced Communications, Villanova University, Villanova, PA, USA. His current research interests include millimeter-wave imaging and radar indoor monitoring.

Shang-Yi Sun (Graduate Student Member, IEEE) received the bachelor's degree and the master's degree from Xidian University, Xi'an, China, in 2016 and 2019, respectively. He is currently pursuing the Ph.D. degree with the Global Big Data Technologies Centre (GBDTC), University of Technology Sydney, Sydney, NSW, Australia. His research interests include multi-band shared-aperture antenna arrays and base-station antennas.

He was a spotlighted student and young professional at the IEEE Foundation Day in 2025. He was a recipient of the 2024 IEEE Antennas and Propagation Society C. J. Reddy Travel Grant for Graduate Students, and the Best Antenna Paper Award at the 2023 IEEE International Symposium on Antennas and Propagation.

Chunyang Teng received the B.S. degree in Communication Engineering from Minzu University of China , Beijing, China, in 2021. She is currently pursuing the Ph.D. degree at the School of Integrated Circuits and Electronics, Beijing Institute of Technology, Beijing, China. Her research interests include array design and near-field imaging.

Guoqiang Zhao received the B.S. and M.S. degrees in electrical engineering and the Ph.D. degree in electromagnetic field and microwave technology from the Beijing Institute of Technology, Beijing, China, in 1994, 2004, and 2013, respectively. He is currently an Associate Professor with the School of Information and Electronics, Beijing Institute of Technology. He is also with the Tangshan Research Institute of BIT, Tangshan 063007, China. His research interests include radar signal processing, polarimetric information processing, microwave/millimeter-wave circuits and systems, and multipolarimetric antenna.

Houjun Sun received the Ph.D. degree in communication and electronic systems from the Beijing Institute of Technology (BIT), Beijing, China, in 1997. He is currently a Professor with BIT, where he is the Director of the Institute of Microwave Technology and the Beijing Key Laboratory of Millimeter Wave and Terahertz Technology. He is also with the Tangshan Research Institute of BIT, Tangshan 063007, China.

His current research interests include the integration and application of the millimeter-wave and terahertz communication systems, active antenna arrays, and millimeter-wave imaging.